Solid State Science and Technology, Vol. 26, No 2 (2018) 85-91
ISSN 0128-7389 | *http://myjms.mohe.gov.my/index.php/masshp*

$Cu_2Zn_{1-x}Cd_xSnS_4$ QUINTERNARY ALLOYS NANOSTRUCTURES DEPOSITED ON POROUS SILICON BY SOL–GEL SPIN COATING TECHNIQUE

A.S. Ibraheam, Y. Al-Douri, U. Hashim

Institute of Nano Electronic Engineering,
University Malaysia Perlis UniMAP, 01000 Kangar, Perlis, Malaysia

Corresponding author: yaldouri@yahoo.com

ABSTRACT

The obtained results are in good agreement with experimental and theoretical data $Cu_2Zn_{1-x}Cd_xSnS_4$ nanostructures with different Zn and Cd contents were grown by a sol-gel method on porous silicon (63.93%.) substrate. The obtained $Cu_2Zn_{1-x}Cd_xSnS_4$ nanostructures/PS (63.93%) products were investigated by Field Emission-Scanning Electron Microscope (FE-SEM), X-ray diffraction (XRD).

Keywords: Nanostructure; Quinternary Alloys; Porous silicon

INTRODUCTION

A kesterite Cu_2ZnSnS_4 (CZTS) is a potential absorber material as thin film solar cells for naturally abundant elements, inexpensive and efficient and environmentally friendly such as Zn and Sn. It is known that CZTS has a direct band gap between 1.45 and 1.6 eV with a high absorption coefficient of over 104 cm^{-1} in visible light, intrinsic p-type conductivity and low thermal conductivity [1–3]. Therefore, these properties promote CZTS as potential candidate for photovoltaic materials. The theoretical predicted efficiency of CZTS based solar cell is larger than 30% [4–7]. Efficiency up to 6.77% has been already reached in solar cells produced with CZTS as absorber layer [8].

Silicon substrates have high quality single crystal with nearly defect free, very low volume density of impurities and controlled amount of dopants. It may be prepared flat on the atomic scale by standard methods that lead to porous silicon (PS) formation arises from a specific process [9]. The porous silicon (PS) Porous Si (PS) is attractive in solar cell applications due to its efficient Antireflection Coatings and other properties such as band gap broadening, wide absorption spectrum and optical transmission range (700–1000 nm). It can also be used for surface passivation and texturization [10-13]. The potential advantages of PS as an Antireflection Coatings for solar cells include surface passivation and removal of the dead layer diffused region. Moreover, PS could convert higher energy solar radiation into spectrum light, which is absorbed more efficiently into bulk Si [14]. Daranfed et al. [4] have observed the PS in the electro

polishing experiments using an electrolyte solution comprising hydrofluoric acid. They have found that the high surface area of PS gives useful model for crystalline silicon surfaces in spectroscopic studies [15-17]. Al-Douri et al. [18] have calculated using empirical pseudo potential method (EPM), the energy gap of Si, which is found to be indirect. They have investigated features such as refractive index, optical dielectric constant, bulk modulus, elastic constants and short-range Ease of Use force constants, in addition to the shear modulus, Young's modulus, Poisson's ratio and Lame's constants for both Si and PS. They have found that the Debye temperature of PS is estimated from the average sound velocity. Hong and Kim [19] have fabricated Cu_2ZnSnS_4 (CZTS) film by sulfurization of two stacked layers of Cu (Zn, Sn) (CZT) alloy precursors. The sulfurization was performed in an evacuated and sealed quartz ampoule with sulfur powder, in which samples were annealed at 450°C, 500°C, or 550°C for 1 h and then allowed to cool naturally. The XRD patterns of all samples are well matched to those of the CZTS crystal. In this study, it is confirmed that the Sn in the metal precursors is lost in the form of SnS gas and a SnS_2 solid that crystallizes upon the combination of SnS and S when the CZTS film is annealed. The band gap energy of CZTS absorber was determined to be 1.370–1.414 eV. The surface morphology and grain shapes of these CZTS thin films were analyzed using SEM images and XRD patterns. Xinkun et al. [20] have deposited Sn/Cu/ZnS precursor using evaporation on soda lime glass at room temperature, and then polycrystalline thin films of Cu_2ZnSnS_4 (CZTS) were produced by sulfurizing the precursors in a sulphur atmosphere at a temperature of 550 °C for 3 h. Fabricated CZTS thin films were characterized by X-ray diffraction, energy dispersive X-ray spectroscopy, ultraviolet-visible-near infrared spectrophotometry, the Hall effect system, and 3D optical microscopy. The experimental results show that, when the ratios of [Cu]/([Zn] + [Sn]) and [Zn]/[Sn] in the CZTS are 0.83 and 1.15, the CZTS thin films possess an absorption coefficient of larger than 4.0×10^4 cm^{-1} in the energy range 1.5–3.5 eV, and a direct band gap of about 1.47 eV. The carrier concentration, resistivity and mobility of the CZTS film are 6.98×10^{16} cm^{-3}, 6.96 Ωcm, and 12.9 $cm^2/(VS)$, respectively and the conduction type is p-type. Therefore, the CZTS thin films are suitable for absorption layers of solar cells. Accordingly, successful experiments have discovered electrochemical and chemical dissolution enable the silicon wafers to emit light in red luminescence [21]. During the last years, the optical properties of PS have become a very intense area of research.

Study the effect of changing the etching parameters and very low current to explore uniformed PS. on the structural properties of these semiconductors. Select optimal etching parameters that control size and shape of nanostructures by modifying current density, etching time and deposited CZSCT on the selected optimal etching parameters and study the characterization, analysis, properties.

EXPERIMENTAL

Sol–gel spin coating technique is used to deposit the $Cu_2Zn_{1-x}Cd_xSnS_4$ quaternary alloy nanostructures onto process silicon substrate. Porous silicon substrate prepared as reported in literature [22], but the process of etching time is 30, 60 and 120 min and the current density is 5 mA/cm^2 DC. First solution of $Cu_2Zn_{1-x}Cd_xSnS_4$ precursors was prepared from copper (II) chloride dehydrate (0.3M), zinc (II) chloride dehydrate (0.3M), tin (II) chloride dehydrate, cadmium (II) chloride (0.3M), thiourea (0.6) was dissolved in 2-methoxyethanol and monoethanolamine (MEA) was added as a stabilizer. The mole ratios of Cu, (Zn + Cd), Sn, and S in the solution are 2:1:1:4. For obtaining the solution with different Cd content (x), the mole ratios of Cd to (Zn +Cd) in the solution vary according to the value of x as 0, 0.6 and 1. The solution was stirred at 50 °C to completely dissolve the metal compounds during stirring the milk solution became a yellow. After that, the solution was dropped onto optimal etching substrate that was rotating at 2500 rpm for 30 sec. After deposition by spin coating, the nanostructures were dried at 250 °C for 80 min on hot plate. The coating and drying processes were repeated for seven times to obtain 1μm thickness.

RESULTS AND DISCUSSION

Different mechanisms of Si dissolution have been presented. It is accepted that holes are required for pores formation. During this formation, two hydrogen atoms enrolled for every dissolved Si atom [23,24]. Current efficiencies are about two electrons per dissolved Si atom of pore formation [24-16]. The final chemical expression can be written during pore formation as:

$$Si+6HF \rightarrow H_2SiF_6 + H_2 + 2H+ + 2e^- \quad (1)$$

According to Bomchil et al. [16], Schottky barrier can be created between the semiconductor and the electrolyte, where the Fermi level is occurred at the Si/electrolyte interface. The reduction of Schottky barrier height is attributed to the generated electric field dissolves the pore tips. Scanning electron microscope (SEM) is a very important to evaluate the porosity percentage fabricated by different methods as gravimetric [27] and image processing [28]. Our results are carried out using gravimetric method,

$$P(\%)=(m1-m2)/(m1-m3) \quad (2)$$

where m1 is the sample weight before etching process, m2 is the weight after etching and m3 is the sample weight after removing the PS layer with 3% KOH or 20% NaOH solution. A summary of the structural characteristic of PS at different etching time and fixed current density is given in Table 1. As the etching time increases, the porosity increases with fixed ethanol ratio.

Table 1: Etching time, ratio and etching current density correspond to porosity percentage.

Etching Time (min.)	**(HF:ethanol) ratio**	**Etching current density (mA /cm^2)**	**Porosity (%)**
30	1:4	5	9.47
60	1:4	5	33.39
120	1:4	5	63.93

Structural properties

The X-ray diffraction (XRD) patterns of $Cu_2Cd_xZn_{1-x}SnS_4$ quinternary alloy nanostructures with x= 0, 0.6 and 1 deposited on PS prepared at the current density of 5 mA/cm^2 for 120 min are shown in Fig. 1 The major diffraction peaks appear at 2θ = 28.757°, 33.313° and 47.30° which can be attributed to the (112), (200), and (220) planes of kesterite phase of Cu_2ZnSnS_4 (ICDD PDF2008, 01-075-4122) and stannite phase of Cu_2CdSnS_4 (ICDD (PDF2008).(00-029-0537). shows the enlarged view of the (112) diffraction peak and increased intensity with Cd content. The peaks are shifted to the lower angle side with increasing Cd content in the CZCTS solid solutions, which was attributed to the increasing lattice spacing. This was due to the fact that the radius of the Cd ion, (1.53 Å), is larger than that of Zn, (1.33 Å), and is supported by previous results [29]. The simplest possibility is that Cd substitutes other metal metals at their sites in crystal lattice of $Cu_2Cd_xZn_{1-x}SnS_4$ quinternary alloy nanostructures. As the theoretically calculated substitution energies of Cd atoms at Cu, Sn and Zn atom sites in CZTS lattice are E_{sub} (CdCu) = 0.69 eV, E_{sub} (CdSn) = 1.07 eV and E_{sub}(CdZn) = 0.53 eV [30], the most likely is the isoelectronic substitution of Cd at the Zn site. Lattice constants a and c were calculated from XRD data for the (112) plane, and are given in Table 2 by using.

$$(1/d^2) = (h^2+k^2)/a^2) + (l^2/c^2), \quad (3)$$

where hkl are the Miller indices, a and c are the lattice constants, and the interplane distance (d) were calculated for all of the CZCTS nanostructures using Bragg's diffraction equation [29].

$$d = h\lambda/2\sin\theta, \quad (4)$$

where λ is wavelength of XRD using (λ=1.5406 Å) and θ is the Bragg's angle.
The crystallite size (D) was calculated by Scherrer's formula [29]

$$D = k\lambda/\beta\cos\theta, \quad (5)$$

Table 2: The structural properties of $Cu_2Zn_{1-x}Cd_xSnS_4$ quinternary alloy nanostructures.

Peak (θ)	Particle size (nm)	dhkl (112) (Å)	Lattice constants a and c (Å)
28.757	30.71	3.46	a= 5.429 c= 10.856
28.736	41.80	3.558	c=5.525 a=10.906
28.723	53.52	3.703	a=5.586 c=11.389

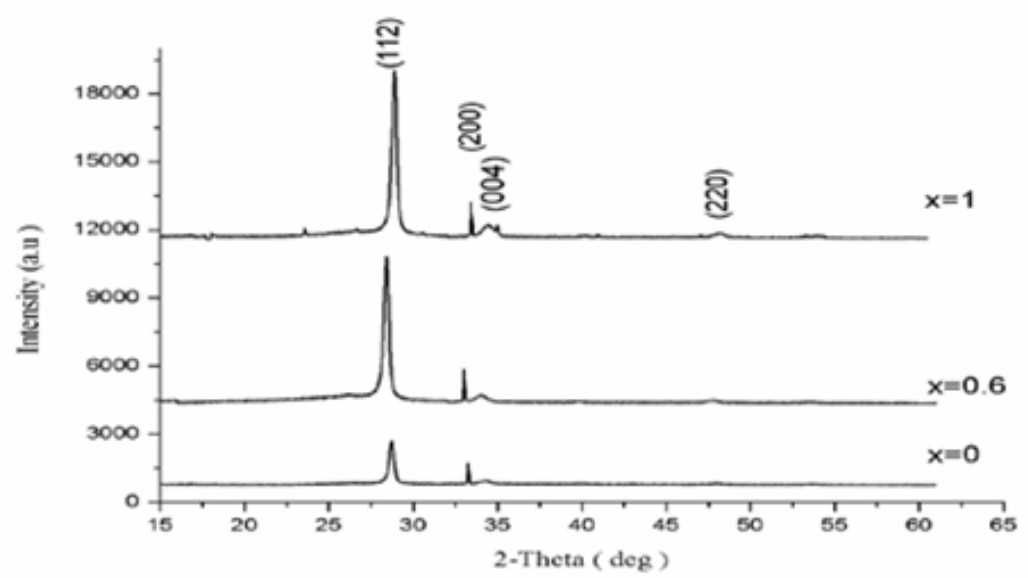

Figure 1: XRD patterns of $Cu_2Zn_{1-x}Cd_xSnS_4$ quinternary alloy nanostructures with different Cd contents, x=0, 0.6,1

Figure 2 shows top-view of FE-SEM images of $Cu_2Zn_{1-x}Cd_xSnS_4$ quinterary alloy nanostructures grown on PS (63.93%) with different Cd content (x). At x=0, the surface has multiple pores among the grains. The number of pores decreases as the Cd content increases. The sample grown with x=0.6 clearly to show the largest grain size. This is because of the adjacent $Cu_2Zn_{1-x}Cd_xSnS_4$ grains are tended to merge into larger ones as Cd content increases. Contrary, at x=1, the grains have extremely small pores. In addition, the top-view image of as prepared n-PS/$Cu_2Zn_{1-x}Cd_xSnS_4$ reveals a uniform distribution of pores, which has been duly filled with $Cu_2Zn_{1-x}Cd_xSnS_4$ quaternary alloy nanostructures.

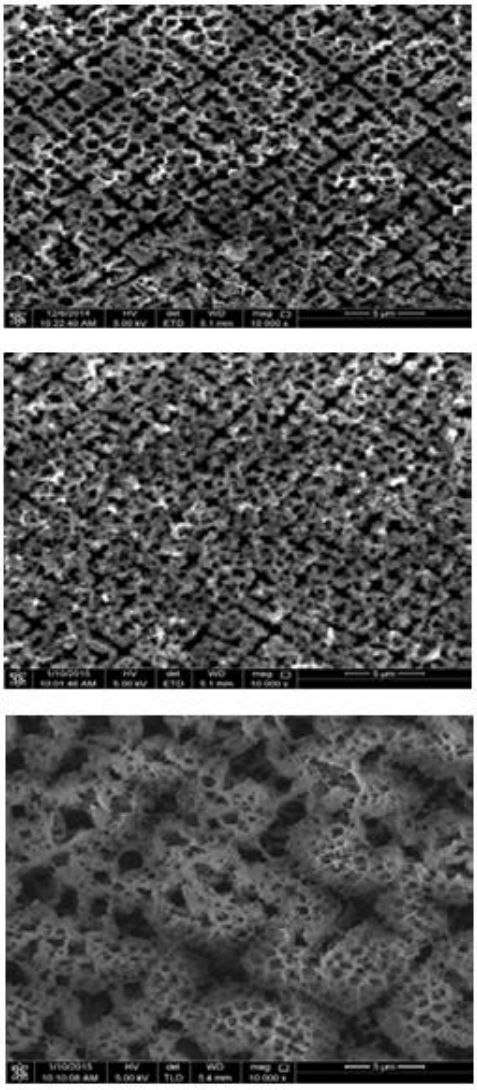

Figure 2: FE-SEM images of $Cu_2Zn_{1-x}Cd_xSnS_4$ quinternary alloy nanostructure grown on PS at different Cd contents, x= 0, 0.6, 1

CONCLUSION

The $Cu_2Zn_{1-x}Cd_xSnS_4$ quinternary alloys nanostructures are grown on n-PS (63.93%) using spin coating technique. The morphological studies via FE-SEM. The number of pores decreases as the Cd content increases. It is found that the largest grain size of $Cu_2Zn_{0.4}Cd_{0.6}SnS_4$ quinternary alloy nanostructure.

REFERENCES

[1] H. Katagiri, K. Saitoh, T. Washio, H. Shinohara, T. Kurumadani, S. Miyajima, *Sol. Energy Mater. Sol. Cells* **65** 141–148 (2001)
[2] N. Kamoun, H. Bouzouita, B. Rezig, *Thin Solid Films* **515** 5949–5952 (2007)
[3] S. Levcenco, D. Dumcenco, Y.P. Wang, Y.S. Huang, C.H. Ho, E. Arushanov, V. Tezlevan, K.K. Tiong, *Opt. Mater.* **34** 1362–1365 (2012)
[4] W. Daranfed, M.S. Aida, N. Attaf, J. Bougdir, H. Rinnert. *Journal of Alloys and Compounds* **542** 22–27 (2012)
[5] T.K. Todorov, K.B. Reuter, D.B. Mitzi, *Adv. Mater.* **22** E156–E159 (2010)
[6] Q.J. Guo, H.W. Hillhouse, R. Agrawal. *J. Am. Chem. Soc.* **131** 11672–11673 (2009)
[7] H. Katagiri, K. Jimbo, W. Shwe Maw, K. Oishi, M. Yamazaki, H. Araki, *Thin Solid Films* **517** 2455–2460 (2009)
[8] L. T. Canham, Properties of Porous Silicon, (Malvern, Dera, UK, 1997)
[9] V.Y. Yerokhov, I.I. Melnyk, *Renew. Sustainable Energy Rev.* **3** 291-299 (1999)
[10] L. Schirone, G. Sotgiu, M. Montecchi, A. Parisini, *Proc. 14th European PV Solar Energy Conf.*, 1997, p.1479
[11] P. Menna, G.D. Francia, V.L. Ferrara, *Solar Energy Mater. Solar Cells* **3** 291-299 (1999)
[12] L. Schirone, G. Sotgiu, M. Montecchi, G. Righini, R. Zanoni, Proc. 2nd World Conf. PV Solar Energy Conversion, 1998, p. p. 276
[13] R.B. Cláudia, R.B. Maurício, F.B. Antonio, G.F. Neidenêi, *J. Braz. Chem. Soc.* **19** 76-82 (2008)
[14] P. Panek, M. Lipinski, H. Czternastek, *Opto-Electron. Rev.* **8** 75-79 (2000)
[15] G. Bomchill, A. Halimaoui, R. Herino, *Microelectronic Eng.* **8** 293-310 (1988)
[16] G. Bomchil, A. Halimaoui, R. Herino, *Appl. Surf. Sci.* **41/42** 604-613 (1990)
[17] R. C. Anderson, R. S. Muller, C. W. Tobias, *Sensor and Actuators A* **23** 835-839 (1990)
[18] Y. Al-Douri, N. M. Ahmed, N. Bouarissa, A. Bouhemadou. *Materials and Design* **32** 4088-4093 (2011)
[19] Hong, Sungwook; Kim, Chan, *Molecular Crystals and Liquid Crystals* **602** 134-143 (2013)
[20] W. Xinkun, L. Wei, C. Shuying, Cheng; Yunfeng, *Journal of Semiconductors* **3** 22002- 22005 (2012)
[21] L. T. Canham, *Appl. Phys. Lett.* **57** 1046-1048 (1990)
[22] Asmiet Ramizya, Z. Hassana, Khalid Omar, Y. Al-Douri , M.A. Mahdi. *Applied Surface Science* **257** 6112–6117 (2011)
[23] C. Pickering, M. I. J. Beale, D. J. Robbins, P. J. Pearson, R. Greef, *J. Phys. C* **17** 6535-6552 (1984)
[24] M. J. Eddowes, *J. Electroanal. Chem.* **280** 297-301 (1990)
[25] M. I. J. Beale, J. D. Benjamin, M. J. Uren, N. G. Chew, A. G. Cullis, *J. Crystal Growth* **73** 622-636 (1985)
[26] V. Lehmann, H. Foll, *J. Electrochem. Soc.* **137** 653-659 (1990)